



Cite this: *Phys. Chem. Chem. Phys.*,
2024, 26, 25005

Elucidation of the exchange interaction in photoexcited three-spin systems – a second-order perturbational approach

Michael Franz, ^a Frank Neese* ^b and Sabine Richert ^{*a}

Photogenerated three-spin systems show great potential for applications in the field of molecular spintronics. In these systems, the exchange interaction in the electronically excited state dictates their magnetic properties. To design such molecules for specific applications, it is thus important to understand how the sign and magnitude of the exchange interaction can be controlled. For this purpose, we developed a perturbational approach, based on previous work by the groups of de Loth and Malrieu, that allows for the direct calculation of the exchange interaction and its individual contributions up to the second order and implemented it within the ORCA program package. Within this manuscript, we present the derivation of the individual second-order contributions, provide an overview of the implementation of the code and illustrate its performance. We show that, using this perturbational approach in combination with state-averaged orbitals from minimal active space calculations, accurate values for the exchange interaction can be computed for organic nitroxides. Further, we demonstrate that the weight of the ionic determinants in the orbital optimisation of the CASSCF procedure is crucial for the computation of accurate exchange couplings. In the case of photoexcited chromophore–radical systems, we find that the dynamic spin polarisation effect constitutes the most important contribution to the exchange interaction, whereby the sign of this contribution determines the sign of the exchange interaction.

Received 30th August 2024,
Accepted 9th September 2024

DOI: 10.1039/d4cp03402c

rsc.li/pccp

1 Introduction

Photoexcited organic multi-spin systems prove to be highly promising candidates for applications in the field of molecular spintronics.^{1–3} This research area aims to utilise the magnetic moment in molecular systems specifically for information processing and data storage.⁴ A noteworthy advantage of photo-generated organic multi-spin systems is their capability to be activated externally through light excitation, facilitating external control over their functionality.^{5–10} Moreover, their excited states are distinguished by spin coherence times that have the potential to exceed those of any metal-containing analogues, thereby enabling functionality close to room temperature.^{11,12}

A prominent example for such organic multi-spin systems are chromophore–radical systems, which typically comprise a chromophore (such as perylene or anthracene) covalently bound to a radical moiety (such as a nitroxide). Chromophore and radical may either be linked directly or *via* a molecular bridge (for example, a phenyl group), which makes these compounds

structurally highly modifiable and provides the opportunity to tailor these structures to specific applications.^{1,13–15} In the simplest case, such systems represent three-spin systems in their excited state, which will be the focus of this manuscript.

The photophysical mechanism underlying the generation of a three-spin system is illustrated in Fig. 1. The chromophore undergoes light excitation from its ground state S_0 to an excited singlet state S_1 . Among other possible concurrent processes (electron transfer, excitation energy transfer, internal conversion, fluorescence), the excited singlet state transitions to a triplet state T_1 *via* intersystem crossing. Due to the coupling between the chromophore singlet and the radical doublet states, this transition is partially allowed and the process is then referred to as enhanced intersystem crossing (EISC). The resulting coupled triplet–doublet system can manifest either as a doublet-coupled system or a quartet-coupled system, depending on the energetic gap and arrangement dictated by the exchange interaction J_{TR} between the chromophore triplet state and the radical doublet state.^{5,16–18}

Since the phenomenological exchange interaction J_{TR} dictates the magnetic properties of these systems,^{1,5} the motivation is to determine the factors that determine its magnitude and sign and how these factors can be influenced by structural modifications.

^a Institute of Physical Chemistry, University of Freiburg, Albertstraße 21, 79104 Freiburg, Germany. E-mail: sabine.richert@physchem.uni-freiburg.de

^b Max-Planck-Institut für Kohlenforschung, Kaiser-Wilhelm-Platz 1, 45470 Mülheim an der Ruhr, Germany. E-mail: neese@kofo.mpg.de



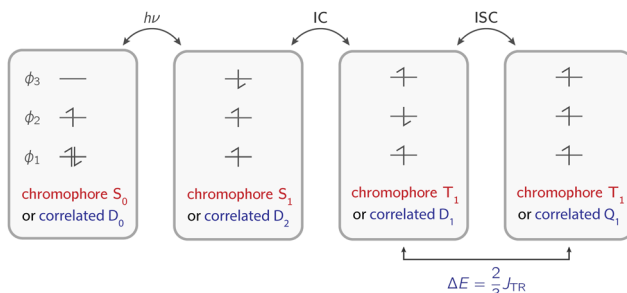


Fig. 1 Schematic representation of the photophysical mechanism. The wavefunctions ϕ_1 , ϕ_2 , and ϕ_3 represent the chromophore HOMO, radical SOMO and chromophore LUMO, respectively. Abbreviations: IC – internal conversion; ISC – intersystem crossing; J_{TR} – exchange interaction between chromophore triplet state T and stable radical R. Note that the orbitals are represented in a canonical basis to ensure a more common picture of the energetic separation of the orbitals.

Especially for exchange interactions arising from the electronically excited state, it can be difficult to determine an exact value through experimental methods, such as transient continuous wave electron paramagnetic resonance spectroscopy (trEPR).^{1,19} Theoretical methods are particularly advantageous in this case, as they allow for the direct calculation or extraction of exchange interactions. Additionally, the exchange interaction can be analysed in detail, enabling a systematic correlation with structural factors.^{20,21}

An important step in this direction was the pioneering work of de Loth *et al.*,²² where second-order perturbation theory was used to identify the classes of determinants in the first-order interacting space (FOIS) that significantly contribute to the exchange interaction. The most crucial aspect of this work was the demonstration that only a small portion of the FOIS is necessary for the calculation of the exchange interaction, as proven theoretically in an earlier work by Malrieu *et al.*²³ Building on these early works, a variational method was developed by Miralles *et al.*, that incorporates only those determinants into the CI space, which have an influence on excitation energies. This is the so-called difference-dedicated configuration interaction method (DDCI),^{24,25} which generally provides the most accurate results for the exchange interaction. However, such a high-level method is only practical for relatively small systems as the DDCI space increases as $N_{\text{CAS}}N^3$, where N is the number of basis functions and N_{CAS} is the dimension of the active space.²¹ Perturbational approaches based on CASSCF zeroth-order wavefunctions, such as the n-electron valence state perturbation theory method (NEVPT2)^{26–28} by Angeli *et al.* or the complete active space perturbation theory method (CASPT2)²⁹ by Andersson *et al.*, offer viable alternatives as they can also be applied to larger systems. Especially the NEVPT2 method has the great advantage of being intruder-state free. However, when using either of these two methods, the individual contributions of two different effects, namely the dynamic spin polarisation effect and the dynamic charge polarisation effect, cannot be extracted.²¹ The relevance of being able to resolve these two contributions prompted us to implement a “difference-dedicated perturbation theory” method based on the work of de Loth *et al.*, which allows (i) the calculation

of the individual contributions of the dynamic spin and charge polarisation effects, and, when combined with SA-CASSCF orbitals, (ii) the calculation of accurate exchange interactions for systems of medium to large size, where DDCI calculations are unfeasible.

2 Exchange interactions in three-spin systems

The exchange interaction is typically described using the Heisenberg–Dirac–van-Vleck Hamiltonian:^{30–32}

$$\hat{H}^{\text{HDVV}} = - \sum_{i < j} J_{ij} \hat{S}_i \hat{S}_j, \quad (1)$$

where the coupling of two localised spins S_i and S_j is associated with an energy parameterised by J_{ij} . The Landé pattern, associated with the HDVV Hamiltonian, provides the energy difference between two different spin states of the same electronic configuration:³³

$$E(S-1) - E(S) = JS. \quad (2)$$

Thus, the exchange interaction between the chromophore triplet state and the radical doublet state is given by:

$$J_{\text{TR}} = \frac{2}{3}(E_{D_1} - E_{Q_1}), \quad (3)$$

where D_1 is the so-called trip-doublet state, which is described by the coupling of the chromophore triplet state with the radical doublet state, and Q_1 is the quartet ground state.^{34,35}

Now, we assume that the states D_1 and Q_1 can be approximately represented by the following wavefunctions:

$$\psi_{Q_1} = \frac{1}{\sqrt{3}}(|\phi_1\phi_2\bar{\phi}_3\rangle + |\phi_1\bar{\phi}_2\phi_3\rangle + |\bar{\phi}_1\phi_2\phi_3\rangle), \quad (4)$$

$$\psi_{D_1} = \frac{1}{\sqrt{6}}(|\phi_1\phi_2\bar{\phi}_3\rangle + |\bar{\phi}_1\phi_2\phi_3\rangle - 2|\phi_1\bar{\phi}_2\phi_3\rangle). \quad (5)$$

where the indices 1, 2, and 3 represent the three electrons. For these states, the following expectation values are obtained:

$$E_{Q_1} = \frac{-J_{12} - J_{13} - J_{23}}{4}, \quad (6)$$

$$E_{D_1} = \frac{2J_{12} + 2J_{23} - J_{13}}{4}. \quad (7)$$

Substituting these into eqn (3), we obtain:

$$J_{\text{TR}} = \frac{J_{12} + J_{23}}{2} \quad (8)$$

This means that the exchange interaction between the chromophore triplet state and the radical doublet state can be approximately represented by two two-electron problems, where the exchange parameters J_{12} and J_{23} represent the interaction between a spin localised at the chromophore HOMO or LUMO (ϕ_1 or ϕ_3) and a spin localised at the radical SOMO ϕ_2 . This approximation becomes exact if $J_{12} = J_{23}$.²⁰ Since J_{13} is expected to be much larger than the difference between J_{12} and J_{23} , it is



reasonable to state that $J_{12} \approx J_{23}$, which justifies the above approximation.

To determine which (structural) factors affect the phenomenological exchange interaction J_{TR} , an analysis must be conducted to identify the factors influencing the individual exchange interactions. As noticed by Malrieu, *et al.*,²³ the individual exchange interactions can be rationalised using a perturbative approach, analogous to the perturbation of the energy difference between a triplet and a singlet state of the same electronic configuration. This procedure was first used by de Loth, *et al.* to calculate the singlet-triplet splitting in the cupric acetate hydrate dimer²² and led to a series of papers also using this technique for the calculation of the singlet-triplet splitting.^{36–39}

Here, we will use this approach to calculate J_{TR} directly as the sum of two individual exchange couplings J_{ij} . To this end, we will derive a modified variant of the previously published method, which will allow us to manipulate the accuracy of the calculated J_{ij} by performing state-averaged CASSCF calculations.

3 Derivation of the second-order contributions to the exchange interaction

3.1 Difference dedicated perturbation theory *versus* difference dedicated configuration interaction

We will illustrate the principles of our approach by first discussing the well-known case of two interacting $S = 1/2$ systems.

The discussion starts with the definition of the model space:

$$\mathbb{S}_0 = \{|\phi_t \bar{\phi}_u\rangle, |\phi_u \bar{\phi}_t\rangle\}, \quad (9)$$

It is important to note, that, in the above Slater determinants, the internal and virtual orbitals ϕ_i, \dots, ϕ_f and ϕ_a, \dots, ϕ_b were ignored for simplicity. For the further discussion, we define the general orbital indices to be p, q , the internal orbital indices to be i, j , the active (magnetic) orbital indices to be t, u, v and the virtual orbital indices to be a, b .

We assume the molecular orbitals ϕ_t and ϕ_u to be of a localised nature. Thus the references space consists of the two neutral $M_s = 0$ determinants. This is the same reference space as in the DDCI2 method⁴⁰ (difference-dedicated configuration interaction with two degrees of freedom) and is an excellent starting point for developing the treatment of exchange couplings. The arguments are based on perturbation theory, which is valid when the ionic contributions in the respective wavefunctions play only a small (but still decisive) role.^{33,41–50} In the DDCI2 method, parts are picked from the first-order-interacting space (FOIS) and ordered according to their “degrees of freedom”. A degree of freedom in this context is either a hole in the doubly occupied orbital space or a particle in the virtual orbital space. The DDCI2 method is rooted in the original and pioneering work of de Loth *et al.* who used perturbation theory to demonstrate which parts of the FOIS contribute in which way to the final exchange couplings.²² In DDCI2, these FOIS functions and their interaction with the reference determinants are treated variationally, which

gives the method increased robustness but also leads to elevated computational cost due to the iterative nature of the configuration interaction problem and the necessity to store integrals and several copies of the wavefunction amplitudes.

An alternative method, where perturbation theory is carried through not only conceptually but also numerically is a continuation of the work of de Loth *et al.* In this work we will refer to it as “difference-dedicated perturbation theory” (DDPT2). The acronym emphasizes that the treatment is based on the same subspace of the FOIS as the original DDCI2 method but that perturbation theory is used for the numerical evaluation of the exchange coupling constants.

3.2 Elaboration of the DDPT equations

The full Hamiltonian \hat{H} is defined as:

$$\hat{H} = \sum_n^N \hat{h}(n) + \sum_{n=1}^{N-1} \sum_{m=1}^N \frac{1}{r_{nm}}, \quad (10)$$

where $\hat{h}(n)$ is the one-electron operator acting on the n 'th electron and $\sum_{n=1}^{N-1} \sum_{m=1}^N \frac{1}{r_{nm}}$ accounts for the two-electron interactions. The eigenfunctions of the electronic Hamiltonian \hat{H} in the aforementioned model space are a triplet wavefunction and a singlet wavefunction:

$$\psi_T = \frac{1}{\sqrt{2}}(|\phi_t \bar{\phi}_u\rangle - |\phi_u \bar{\phi}_t\rangle), \quad (11)$$

$$\psi_S = \frac{1}{\sqrt{2}}(|\phi_t \bar{\phi}_u\rangle + |\phi_u \bar{\phi}_t\rangle). \quad (12)$$

The energy difference between the two wavefunctions, which is of primary interest, is given by:

$$\Delta E_{S \rightarrow T} = E_S - E_T = J_{tu} = 2K_{tu}. \quad (13)$$

This constitutes the result up to the first order. Due to the fact that the exchange integral K_{tu} is always positive, only the ferromagnetic coupling of two spins can be described within the model space defined above. This is necessarily an incomplete description, as an anti-ferromagnetic coupling between two spins can also occur.⁵⁰ One way of describing the coupling of two spins in a better way is to perturb the triplet state and the singlet state up to the second order.²² For this, we will define the zeroth-order Hamiltonian $\hat{H}^{(0)}$ as the sum of the CASSCF Fock-type operators:^{51,52}

$$\hat{H}^{(0)} = \sum_n \hat{F}_n, \quad (14)$$

which is assumed to be diagonal within the full space $\mathbb{S} = \mathbb{S}_0 + \mathbb{S}_r$, where \mathbb{S}_r includes all excited state determinants. The matrix elements of the Fock-type operator are given by:

$$F_{pq} = F_{pq}^{\text{inactive}} + F_{pq}^{\text{active}}, \quad (15)$$

where F_{pq}^{inactive} corresponds to the inactive part of the Fock operator:

$$F_{pq}^{\text{inactive}} = h_{pq} + 2 \sum_i [(pq|ii) - 1/2(pi|qi)], \quad (16)$$

and F_{pq}^{active} corresponds to the active part of the Fock operator:

$$F_{pq}^{\text{active}} = \sum_{tu} D_{tu}^{\text{av}}[(pq|tu) - 1/2(pt|qu)]. \quad (17)$$

Here, D_{tu}^{av} is the state-averaged first-order reduced density matrix:

$$D_{tu}^{\text{av}} = \sum_I w_I D_{tu}^I, \quad (18)$$

where the first-order reduced density matrices of the states I are weighted by the factor w_I . The state-specific first-order reduced density matrices are given by:

$$D_{tu}^I = \langle I | \hat{E}_{tu} | I \rangle, \quad (19)$$

with $|I\rangle$ being a multi-determinantal eigenstate within the active space and $\hat{E}_{tu} = \sum_{pq} \hat{a}_{pq}^\dagger \hat{a}_{q\sigma}$, where \hat{a}^\dagger and \hat{a} are creation and annihilation operators. σ denotes the spin quantum number. We choose $\hat{H}^{(0)}$ to be the CASSCF Fock-type operator since this implies, that the state-averaging procedure will allow us to influence the extent of the magnetic orbitals ϕ_t and ϕ_u , which should have a significant impact on the exchange coupling.⁵³

The perturbation \hat{V} is then defined to be the difference between the full electronic Hamiltonian and the zeroth-order Hamiltonian:

$$\hat{V} = \hat{H} - \hat{H}^{(0)}. \quad (20)$$

The second-order corrections are defined as follows:

$$E_{\text{T}}^{(2)} = \sum_r \frac{\langle \psi_{\text{T}} | \hat{H} | \psi_r \rangle^2}{E_0^{(0)} - E_r^{(0)}}, \quad (21)$$

$$E_{\text{S}}^{(2)} = \sum_r \frac{\langle \psi_{\text{S}} | \hat{H} | \psi_r \rangle^2}{E_0^{(0)} - E_r^{(0)}}, \quad (22)$$

where the states $|\psi_r\rangle$ are electronically excited states with reference to ψ_{T} and ψ_{S} , and $E_0^{(0)} - E_r^{(0)}$ corresponds to a difference in orbital energies ε according to the definition of $\hat{H}^{(0)}$. Subtracting the second-order corrections from each other, we obtain:

$$\Delta E_{\text{S} \rightarrow \text{T}}^{(2)} = +2 \sum_r \frac{\langle \phi_t \bar{\phi}_u | \hat{H} | \psi_r \rangle \langle \psi_r | \hat{H} | \phi_u \bar{\phi}_t \rangle}{E_0^{(0)} - E_r^{(0)}}, \quad (23)$$

which is $2\Delta K_{tu}^{(2)}$, where $\Delta K_{tu}^{(2)}$ is the second-order correction of the exchange integral. The corrected singlet-triplet gap is then defined as:

$$\Delta E_{\text{S} \rightarrow \text{T}} = 2(K_{tu} + \Delta K_{tu}^{(2)}) = 2K_{tu}^{\text{eff}}. \quad (24)$$

The derived second-order expression assumes that the excited determinants $|\psi_r\rangle$ couple simultaneously with both reference determinants $|\phi_t \bar{\phi}_u\rangle$ and $|\phi_u \bar{\phi}_t\rangle$, leading to a significant reduction of the space of excited determinants. As a consequence, a considerable amount of computation time can be saved.²²

In the following, the excited determinants $|\psi_r\rangle$ will be classified and the corresponding corrections to the exchange integral $\Delta K_{tu}^{(2)}$ will be derived. The possible corrections to the exchange integral K_{tu} include the kinetic exchange, the hole polarisation effect, the particle polarisation effect, the internal \rightarrow active double

excitations, the active \rightarrow virtual double excitations, the dynamic spin polarisation effect, and the dynamic charge polarisation effect.²¹

3.2.1 Kinetic exchange contribution. A well-known second-order effect is the kinetic exchange, where the reference determinants $|\phi_t \bar{\phi}_u\rangle$ and $|\phi_u \bar{\phi}_t\rangle$ are coupled *via* determinants with ionic configurations within the active space. Consequently, the space of excited determinants is defined by $\{|\phi_t \bar{\phi}_t\rangle, |\phi_u \bar{\phi}_u\rangle\}$, which are illustrated in Fig. 2.

The correction of the exchange integral through the kinetic exchange is given by the contributions of two excited state configurations:

$$\begin{aligned} \Delta K_{tu, \text{KE}}^{(2)} = & \frac{\langle \phi_t \bar{\phi}_u | \hat{H} | \phi_t \bar{\phi}_t \rangle \langle \phi_t \bar{\phi}_t | \hat{H} | \phi_u \bar{\phi}_u \rangle}{\Delta E_{u \rightarrow t}} \\ & + \frac{\langle \phi_t \bar{\phi}_u | \hat{H} | \phi_u \bar{\phi}_u \rangle \langle \phi_u \bar{\phi}_u | \hat{H} | \phi_t \bar{\phi}_t \rangle}{\Delta E_{t \rightarrow u}} \end{aligned} \quad (25)$$

Here, we will approximate the off-diagonal terms in the nominator through the CASSCF Fock matrix elements F_{tu} , where only the active part of the Fock matrix might cause a deviation from the corresponding off-diagonal element of \hat{H} . Thus, only a minor deviation should be expected. This leads to a final contribution of:

$$\Delta K_{tu, \text{KE}}^{(2)} = \frac{F_{tu}^2}{J_{tu}^{\text{C}} - J_{tt}^{\text{C}}} + \frac{F_{tu}^2}{J_{tu}^{\text{C}} - J_{uu}^{\text{C}}}. \quad (26)$$

Since ϕ_t and ϕ_u are often nearly degenerate, the denominators are represented by (negative) one-site Coulomb repulsion energies $J_{tu}^{\text{C}} - J_{tt}^{\text{C}}$ and $J_{tu}^{\text{C}} - J_{uu}^{\text{C}}$ instead of the difference of the orbital energies, as would be the case for $\hat{H}^{(0)} = \sum_n \hat{F}_n$. The reason for this is to circumvent the divergence of the perturbational approach. Note that J_{tu}^{C} corresponds to the two-electron integral $\langle tt|uu\rangle$ and J_{tt}^{C} corresponds to $\langle tt|tt\rangle$, whereby the chemist's notation⁵⁴ is used.

As can be seen from the denominator, the kinetic exchange always favours anti-ferromagnetic coupling.

3.2.2 Contribution from internal \rightarrow active single excitations. Another excitation class includes determinants representing single excitations from the internal space to the active space that can be coupled with single excitations within the active space. This excitation class is labelled as "internal \rightarrow active" and is often referred to in the literature as the 1h excitation class, as a hole is created in the internal space. The reference determinants can be coupled *via* four possible types of excited state configurations $\mathbb{S} = \{|\bar{\phi}_i \phi_t \bar{\phi}_t \phi_u\rangle, |\bar{\phi}_i \phi_t \phi_u \bar{\phi}_u\rangle, |\phi_i \phi_t \bar{\phi}_t \bar{\phi}_u\rangle, |\phi_i \bar{\phi}_t \phi_u \bar{\phi}_u\rangle\}$, which are illustrated in Fig. 3.

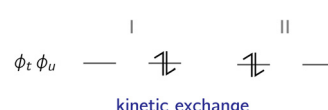


Fig. 2 The kinetic exchange effect stems from the interaction of the ionic forms (I and II) within the active space with the reference determinants (*i.e.* the neutral forms within the active space).

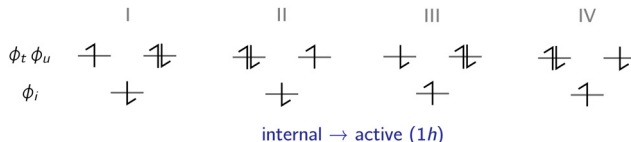


Fig. 3 Four types of configurations can be generated through single excitations from the internal space to the active space considering both reference determinants. These excited determinants are usually referred to as 1h determinants.

This class of excited state determinants leads to the following contributions:

$$\begin{aligned}
 & \sum_i \frac{\langle \phi_i \bar{\phi}_i \phi_t \bar{\phi}_u | \hat{H} | \bar{\phi}_i \phi_t \bar{\phi}_i \phi_u \rangle \langle \bar{\phi}_i \phi_t \bar{\phi}_i \phi_u | \hat{H} | \phi_i \bar{\phi}_i \phi_u \bar{\phi}_t \rangle}{\Delta E_{i \rightarrow u}} \\
 &= \sum_i \frac{-F_{iu} \cdot (tu|ui)}{\varepsilon_i - \varepsilon_u}, \\
 & \sum_i \frac{\langle \phi_i \bar{\phi}_i \phi_t \bar{\phi}_u | \hat{H} | \bar{\phi}_i \phi_t \phi_u \bar{\phi}_u \rangle \langle \bar{\phi}_i \phi_t \phi_u \bar{\phi}_u | \hat{H} | \phi_i \bar{\phi}_i \phi_u \bar{\phi}_t \rangle}{\Delta E_{i \rightarrow t}} \\
 &= \sum_i \frac{-F_{it} \cdot (tu|ti)}{\varepsilon_i - \varepsilon_t}, \\
 & \sum_i \frac{\langle \phi_i \bar{\phi}_i \phi_t \bar{\phi}_u | \hat{H} | \phi_i \bar{\phi}_t \phi_u \bar{\phi}_u \rangle \langle \phi_i \bar{\phi}_t \phi_u \bar{\phi}_u | \hat{H} | \phi_i \bar{\phi}_i \phi_u \bar{\phi}_t \rangle}{\Delta E_{i \rightarrow t}} \\
 &= \sum_i \frac{-F_{iu} \cdot (tu|ti)}{\varepsilon_i - \varepsilon_u}, \\
 & \sum_i \frac{\langle \phi_i \bar{\phi}_i \phi_t \bar{\phi}_u | \hat{H} | \phi_i \bar{\phi}_t \bar{\phi}_u \bar{\phi}_u \rangle \langle \phi_i \bar{\phi}_t \bar{\phi}_u \bar{\phi}_u | \hat{H} | \phi_i \bar{\phi}_i \phi_u \bar{\phi}_t \rangle}{\Delta E_{i \rightarrow t}} \\
 &= \sum_i \frac{-F_{it} \cdot (tu|ui)}{\varepsilon_i - \varepsilon_t},
 \end{aligned} \tag{27}$$

which, in summary, give a total correction of:

$$\Delta K_{tu,1h}^{(2)} = -2 \sum_i \left[\frac{F_{it} \cdot (tu|ui)}{\varepsilon_i - \varepsilon_t} + \frac{F_{iu} \cdot (tu|ti)}{\varepsilon_i - \varepsilon_u} \right], \tag{28}$$

Again, the off-diagonal terms in the nominator, which correspond to single excitations, are approximated by the CASSCF Fock matrix elements.

3.2.3 Contribution from active \rightarrow virtual single excitations. An analogous excitation class comprises excited state determinants generated by single excitations from the active space to the virtual space that can be coupled with single excitations within the active space. This excitation class is labelled as “active \rightarrow virtual” and is frequently referred to in the literature as the 1p excitation class, as a particle is created in the virtual space. The reference determinants are coupled via four types of excited state configurations $\mathbb{S} = \{|\phi_t \bar{\phi}_a\rangle, |\phi_u \bar{\phi}_a\rangle, |\bar{\phi}_u \phi_a\rangle, |\bar{\phi}_t \phi_a\rangle\}$, which are illustrated in Fig. 4.

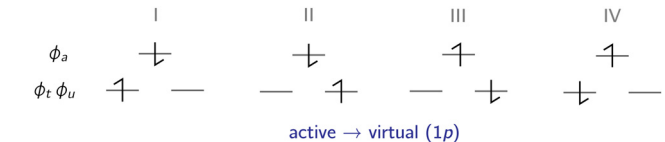


Fig. 4 Analogous to the 1h excitation class, four types of configurations can be generated through single excitations from the active space to the virtual space considering both reference determinants. These excited determinants are usually referred to as 1p determinants.

The 1p determinants yield the following contributions to the exchange integral:

$$\begin{aligned}
 1) \sum_a \frac{\langle \phi_t \bar{\phi}_u | \hat{H} | \phi_t \bar{\phi}_a \rangle \langle \phi_t \bar{\phi}_a | \hat{H} | \phi_u \bar{\phi}_t \rangle}{\Delta E_{u \rightarrow a}} &= \sum_a \frac{F_{ua} \cdot (tu|ta)}{\varepsilon_u - \varepsilon_a}, \\
 2) \sum_a \frac{\langle \phi_t \bar{\phi}_u | \hat{H} | \phi_u \bar{\phi}_a \rangle \langle \phi_u \bar{\phi}_a | \hat{H} | \phi_u \bar{\phi}_t \rangle}{\Delta E_{t \rightarrow a}} &= \sum_a \frac{F_{ta} \cdot (tu|ua)}{\varepsilon_t - \varepsilon_a}, \\
 3) \sum_a \frac{\langle \phi_t \bar{\phi}_u | \hat{H} | \bar{\phi}_u \phi_a \rangle \langle \bar{\phi}_u \phi_a | \hat{H} | \phi_u \bar{\phi}_t \rangle}{\Delta E_{t \rightarrow a}} &= \sum_a \frac{F_{ta} \cdot (tu|ua)}{\varepsilon_t - \varepsilon_a}, \\
 4) \sum_a \frac{\langle \phi_t \bar{\phi}_u | \hat{H} | \bar{\phi}_t \phi_a \rangle \langle \bar{\phi}_t \phi_a | \hat{H} | \phi_u \bar{\phi}_t \rangle}{\Delta E_{u \rightarrow a}} &= \sum_a \frac{F_{ua} \cdot (tu|ta)}{\varepsilon_u - \varepsilon_a},
 \end{aligned} \tag{29}$$

which, in summary, give a total correction of:

$$\Delta K_{tu,1p}^{(2)} = +2 \sum_a \left[\frac{F_{ta} \cdot (tu|ua)}{\varepsilon_t - \varepsilon_a} + \frac{F_{ua} \cdot (tu|ta)}{\varepsilon_u - \varepsilon_a} \right]. \tag{30}$$

As in the case of the 1h excitation class, the single excitation terms in the nominator are approximated by the corresponding CASSCF Fock matrix elements.

All further excitation classes involve only double excitations relative to the reference determinants.

3.2.4 Contribution from internal \rightarrow active double excitations.

One of these excitation classes includes double excitations from the internal space to the active space, denoted as “double internal \rightarrow active” and referred to in the literature as the 2h excitation class. The reference determinants are coupled via a single type of excited configurations $\mathbb{S} = \{|\phi_i \bar{\phi}_j \phi_t \bar{\phi}_i \phi_u \bar{\phi}_u\rangle\}$, illustrated in Fig. 5. This results in the following contribution to the exchange

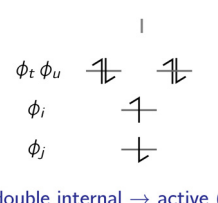


Fig. 5 A single type of configurations can be generated through a double excitation from the internal space to the active space, referred to as a 2h configuration.



integral:

$$\Delta K_{tu,2h}^{(2)} = \sum_i \sum_j \frac{\langle \phi_i \bar{\phi}_u | \hat{H} | \phi_i \bar{\phi}_j \phi_t \bar{\phi}_t \phi_u \bar{\phi}_u \rangle \langle \phi_i \bar{\phi}_j \phi_t \bar{\phi}_t \phi_u \bar{\phi}_u | \hat{H} | \phi_u \bar{\phi}_i \rangle}{\Delta E_{i \rightarrow t} + \Delta E_{j \rightarrow u}} \\ = \sum_i \sum_j \frac{(tj|ui)(uj|ti)}{\varepsilon_i - \varepsilon_t + \varepsilon_j - \varepsilon_u}. \quad (31)$$

This expression includes only bicentric two-electron integrals, with their magnitude depending on the simultaneous differential overlap of ϕ_i and ϕ_j with ϕ_t and ϕ_u . Therefore, it can be assumed that the contribution of this excitation class to the exchange integral is relatively small.

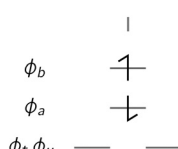
3.2.5 Contribution from active \rightarrow virtual double excitations. A class analogous to the 2h excitation class can be defined by double excitation from the active space to the virtual space. This excitation class is denoted as “double active \rightarrow virtual” and is referred to in the literature as the 2p excitation class. The reference determinants are coupled via one type of excited configurations $\mathbb{S} = \{|\phi_a \bar{\phi}_b\rangle\}$ illustrated in Fig. 6.

The correction to the exchange integral is then given by:

$$\Delta K_{tu,2p}^{(2)} = \sum_a \sum_b \frac{\langle \phi_i \bar{\phi}_u | \hat{H} | \phi_a \bar{\phi}_b \rangle \langle \phi_a \bar{\phi}_b | \hat{H} | \phi_u \bar{\phi}_i \rangle}{\Delta E_{i \rightarrow a} + \Delta E_{u \rightarrow b}} \\ = \sum_a \sum_b \frac{(ta|ub)(ua|tb)}{\varepsilon_t - \varepsilon_a + \varepsilon_u - \varepsilon_b}. \quad (32)$$

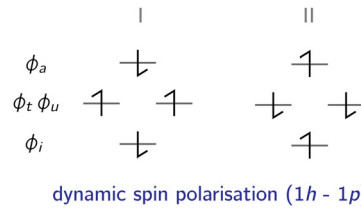
Here, analogous to the 2h excitation class, the magnitude of the correction due to the 2p determinants depends on the simultaneous differential overlap of the outer-space orbitals (ϕ_a and ϕ_b) with the orbitals of the active space ϕ_t and ϕ_u . Therefore, a relatively small contribution of this excitation class to the correction of the exchange integral can be expected.

3.2.6 Contributions from dynamic spin and charge polarisation. The final excitation class is characterised by a single excitation from the internal to the virtual space coupled with a single excitation within the active space. This excitation class is known in the literature as the 1h-1p excitation class. However, two distinct effects can be distinguished in principle: the dynamic spin polarisation effect and the dynamic charge polarisation effect. In the widely used NEVPT2



double active \rightarrow virtual (2p)

Fig. 6 Analogous to the 2h class of excited states, only a single type of configurations can be generated through a double excitation from the active space to the virtual space, referred to as a 2p configuration.



dynamic spin polarisation (1h-1p)

Fig. 7 The dynamic spin polarisation effect describes the coupling of the reference determinants through determinants which exhibit a spin polarisation inside the active space (and inside the outer space). These excited state determinants belong to the 1h-1p excitation class.

(n-electron valence state perturbation theory) method,^{26–28} these effects are jointly calculated within the framework of the 1h-1p (also referred to as $V_{1a}^{(0)}$) excitation class.

The dynamic spin-polarised determinants are generated by coupled triplet excitations, where two different types of excited state determinants $\mathbb{S} = \{|\phi_i \bar{\phi}_t \bar{\phi}_u \phi_a\rangle, |\bar{\phi}_i \phi_t \phi_u \bar{\phi}_a\rangle\}$, which are illustrated in Fig. 7, can interact with the reference determinants.

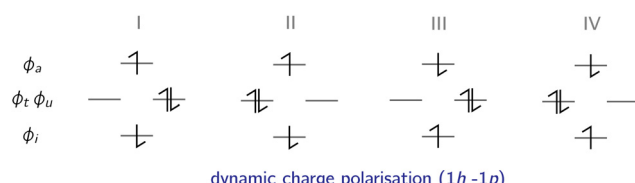
The corresponding contributions to the exchange integral are given by:

$$\sum_i \sum_a \frac{\langle \phi_i \bar{\phi}_u | \hat{H} | \phi_i \bar{\phi}_t \bar{\phi}_u \phi_a \rangle \langle \phi_i \bar{\phi}_t \bar{\phi}_u \phi_a | \hat{H} | \phi_u \bar{\phi}_i \rangle}{\Delta E_{i \rightarrow a}} \\ = \sum_i \sum_a \frac{-(ti|ta)(ui|ua)}{\varepsilon_i - \varepsilon_a}, \\ \sum_i \sum_a \frac{\langle \phi_i \bar{\phi}_u | \hat{H} | \bar{\phi}_i \phi_t \phi_u \bar{\phi}_a \rangle \langle \bar{\phi}_i \phi_t \phi_u \bar{\phi}_a | \hat{H} | \phi_u \bar{\phi}_i \rangle}{\Delta E_{i \rightarrow a}} \\ = \sum_i \sum_a \frac{-(ti|ta)(ui|ua)}{\varepsilon_i - \varepsilon_a}, \quad (33)$$

which, in summary, give a total correction of:

$$\Delta K_{tu,DSP}^{(2)} = -2 \sum_i \sum_a \frac{(ti|ta)(ui|ua)}{\varepsilon_i - \varepsilon_a}, \quad (34)$$

where only monocentric two-electron integrals are included. Hence, a non-negligible contribution can be expected for bridging orbitals ϕ_i and ϕ_a with small energetic separation and large differential overlap. It is known that the sign of



dynamic charge polarisation (1h-1p)

Fig. 8 The dynamic charge polarisation effect describes the coupling of the reference determinants through determinants which exhibit a charge polarisation inside the active space coupled with a single excitation from the internal to the virtual space. These excited state determinants belong to the 1h-1p excitation class.



this effect varies depending on the symmetry of the involved orbitals.^{22,55}

The dynamic charge-polarised determinants are generated by a singlet excitation from the internal space to the virtual space coupled with a singlet excitation within the active space, producing a charge polarisation within the active space. Here, four different types of excited state determinants $\mathbb{S} = \{|\bar{\phi}_i\phi_u\bar{\phi}_u\phi_a\rangle, |\bar{\phi}_i\phi_t\bar{\phi}_t\phi_a\rangle, |\phi_i\phi_u\bar{\phi}_u\bar{\phi}_a\rangle, |\phi_i\phi_t\bar{\phi}_t\bar{\phi}_a\rangle\}$, which are illustrated in Fig. 8, can interact with the reference determinants.

The corresponding contributions are given by:

$$\begin{aligned}
(1) \quad & \sum_i \sum_a \frac{\langle \phi_i \bar{\phi}_u | \hat{H} | \bar{\phi}_i \phi_u \bar{\phi}_u \phi_a \rangle \langle \bar{\phi}_i \phi_u \bar{\phi}_u \phi_a | \hat{H} | \phi_u \bar{\phi}_t \rangle}{\Delta E_{i \rightarrow a} + \Delta E_{t \rightarrow u}} \\
&= \sum_i \sum_a \frac{(tu|ia) \cdot [(tu|ia) - (ui|ta)]}{\varepsilon_i - \varepsilon_a + J_{tu}^C - J_{uu}^C} \\
(2) \quad & \sum_i \sum_a \frac{\langle \phi_i \bar{\phi}_u | \hat{H} | \bar{\phi}_i \phi_u \bar{\phi}_t \phi_a \rangle \langle \bar{\phi}_i \phi_u \bar{\phi}_t \phi_a | \hat{H} | \phi_u \bar{\phi}_t \rangle}{\Delta E_{i \rightarrow a} + \Delta E_{u \rightarrow t}} \\
&= \sum_i \sum_a \frac{(tu|ia) \cdot [(tu|ia) - (ti|ua)]}{\varepsilon_i - \varepsilon_a + J_{tu}^C - J_{tt}^C} \\
(3) \quad & \sum_i \sum_a \frac{\langle \phi_i \bar{\phi}_u | \hat{H} | \phi_i \phi_u \bar{\phi}_u \bar{\phi}_a \rangle \langle \phi_i \phi_u \bar{\phi}_u \bar{\phi}_a | \hat{H} | \phi_u \bar{\phi}_t \rangle}{\Delta E_{i \rightarrow a} + \Delta E_{t \rightarrow u}} \\
&= \sum_i \sum_a \frac{(tu|ia) \cdot [(tu|ia) - (ui|ta)]}{\varepsilon_i - \varepsilon_a + J_{tu}^C - J_{uu}^C} \\
(4) \quad & \sum_i \sum_a \frac{\langle \phi_i \bar{\phi}_u | \hat{H} | \phi_i \phi_u \bar{\phi}_t \phi_a \rangle \langle \phi_i \phi_u \bar{\phi}_t \phi_a | \hat{H} | \phi_u \bar{\phi}_t \rangle}{\Delta E_{i \rightarrow a} + \Delta E_{u \rightarrow t}} \\
&= \sum_i \sum_a \frac{(tu|ia) \cdot [(ti|ua) - (ui|ta)]}{\varepsilon_i - \varepsilon_a + J_{tu}^C - J_{tt}^C}
\end{aligned} \tag{35}$$

As in the case of the kinetic exchange contribution, the energy differences $\Delta E_{t \rightarrow u}$ and $\Delta E_{u \rightarrow t}$ are represented by the one-site repulsion energies instead of the orbital energies, which form the actual ΔE for the chosen $\hat{H}^{(0)}$. These four contributions yield a total correction of:

$$\begin{aligned} \Delta K_{tu, \text{DCP}}^{(2)} &= 2 \sum_i \sum_a \frac{(tu|ia)^2 - (tu|ia)(ui|ta)}{\varepsilon_i - \varepsilon_a + J_{tu}^C - J_{uu}^C} \\ &+ 2 \sum_i \sum_a \frac{(tu|ia)^2 - (tu|ia)(ti|ua)}{\varepsilon_i - \varepsilon_a + J_{tu}^C - J_{ui}^C}, \end{aligned} \quad (36)$$

which, contrary to the dynamic spin polarisation effect, does only involve bicentric two-electron integrals and, thus, may have a smaller contribution to the exchange integral compared to the dynamic spin polarisation effect.

3.2.7 Corrections for the three-electron-three-centre case. So far, all second-order contributions to the exchange integral K_{tu} were discussed for a two-electron-two-centre case. However, in case of a three-electron-three-centre problem, all second-order effects, which involve single

excitations (kinetic exchange, 1h and 1p effect), need to be corrected by incorporating the interaction with a third active orbital ϕ_{ν} .

The kinetic exchange is corrected by including interactions with the excited states shown in Fig. 9: $\mathbb{S}^r = \{|\phi_t\phi_v\bar{\phi}_v\rangle, |\phi_u\phi_v\bar{\phi}_v\rangle, |\phi_t\bar{\phi}_t\phi_u\rangle, |\phi_t\phi_u\bar{\phi}_u\rangle\}$.

The corrections to the exchange integral are given by:

$$\begin{aligned}
 (1) \frac{\langle \phi_t \bar{\phi}_u \phi_v | \hat{H} | \phi_t \phi_v \bar{\phi}_v \rangle \langle \phi_t \phi_v \bar{\phi}_v | \hat{H} | \phi_u \bar{\phi}_t \phi_v \rangle}{\Delta E_{u \rightarrow v}} &= \frac{F_{uv} \cdot (tu|tv)}{J_{uv}^C - J_{vv}^C} \\
 (2) \frac{\langle \phi_t \bar{\phi}_u \phi_v | \hat{H} | \phi_u \phi_v \bar{\phi}_v \rangle \langle \phi_u \phi_v \bar{\phi}_v | \hat{H} | \phi_u \bar{\phi}_t \phi_v \rangle}{\Delta E_{t \rightarrow v}} &= \frac{F_{tv} \cdot (tu|uv)}{J_{tv}^C - J_{vv}^C} \\
 (3) \frac{\langle \phi_t \bar{\phi}_u \phi_v | \hat{H} | \phi_t \bar{\phi}_t \phi_u \rangle \langle \phi_t \bar{\phi}_t \phi_u | \hat{H} | \phi_u \bar{\phi}_t \phi_v \rangle}{\Delta E_{v \rightarrow t}} &= \frac{-F_{tv} \cdot (tu|uv)}{J_{tv}^C - J_{tt}^C} \\
 (4) \frac{\langle \phi_t \bar{\phi}_u \phi_v | \hat{H} | \phi_t \phi_u \bar{\phi}_u \rangle \langle \phi_t \phi_u \bar{\phi}_u | \hat{H} | \phi_u \bar{\phi}_t \phi_v \rangle}{\Delta E_{v \rightarrow u}} &= \frac{-F_{uv} \cdot (tu|tv)}{J_{uv}^C - J_{uu}^C}
 \end{aligned} \tag{37}$$

which yield a total correction of:

$$\begin{aligned} \Delta K_{tu} &= F_{uv} \cdot (tu|tv) \cdot \left[\frac{1}{J_{uv}^C - J_{vv}^C} - \frac{1}{J_{uv}^C - J_{uu}^C} \right] \\ &\quad + F_{tv} \cdot (tu|uv) \cdot \left[\frac{1}{J_{tv}^C - J_{uu}^C} - \frac{1}{J_{tv}^C - J_{tu}^C} \right], \end{aligned} \quad (38)$$

which can be assumed to have only a small contribution because of the cancellation inside the brackets. The single excitation terms are again approximated by the CASSCF Fock matrix elements and the energy differences are chosen to be the corresponding one-site repulsion energies, instead of the orbital energies, which would normally result for the chosen $\hat{H}^{(0)}$

The excited state determinant space of the additional 1h contribution is given by: $\mathbb{S}^r = \{|\phi_i\phi_u\bar{\phi}_u\phi_v\bar{\phi}_v\rangle, |\phi_i\phi_t\bar{\phi}_t\phi_v\bar{\phi}_v\rangle, |\phi_i\phi_t\bar{\phi}_t\phi_u\bar{\phi}_u\rangle\}$. As can be seen in Fig. 10, these excited states are generated by a single excitation from the internal space to the active space coupled with a single excitation within the active space where the additional active orbital ϕ_v is involved.

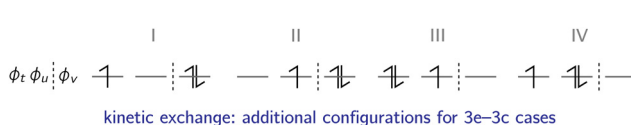
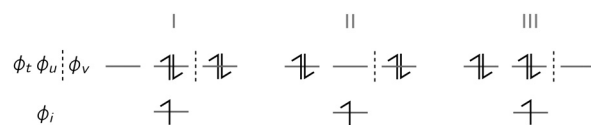


Fig. 9 In the case of a 3c–3e system, four additional ionic configurations within the active space contribute to the kinetic exchange.



1h: additional configurations for 3e–3c cases

Fig. 10 In the case of a 3c-3e system, three additional 1h configurations contribute to the exchange interaction.

Thus, the corrections are given by:

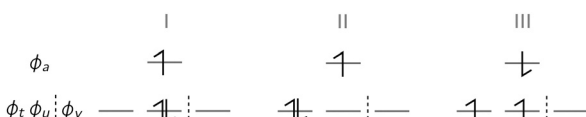
$$\begin{aligned}
 (1) \quad & \sum_i \frac{\langle \phi_i \bar{\phi}_u \phi_v | \hat{H} | \phi_i \phi_u \bar{\phi}_v \phi \bar{\phi}_v \rangle \langle \phi_i \phi_u \bar{\phi}_v \phi_v \bar{\phi}_v | \hat{H} | \phi_u \bar{\phi}_i \phi_v \rangle}{\Delta E_{i \rightarrow v} + \Delta E_{i \rightarrow u}} \\
 &= \sum_i \frac{(tu|vi)^2 - (tu|vi)(tv|ui)}{\varepsilon_i - \varepsilon_v + J_{tu}^C - J_{uu}^C} \\
 (2) \quad & \sum_i \frac{\langle \phi_i \bar{\phi}_u \phi_v | \hat{H} | \phi_i \phi_t \bar{\phi}_i \phi_v \bar{\phi}_v \rangle \langle \phi_i \phi_t \bar{\phi}_i \phi_v \bar{\phi}_v | \hat{H} | \phi_u \bar{\phi}_i \phi_v \rangle}{\Delta E_{i \rightarrow v} + \Delta E_{u \rightarrow t}} \\
 &= \sum_i \frac{(tu|vi)^2 - (tu|vi)(uv|ti)}{\varepsilon_i - \varepsilon_v + J_{tu}^C - J_{tt}^C} \\
 (3) \quad & \sum_i \frac{\langle \phi_i \bar{\phi}_u \phi_v | \hat{H} | \phi_i \phi_t \bar{\phi}_i \phi_u \bar{\phi}_u \rangle \langle \phi_i \phi_t \bar{\phi}_i \phi_u \bar{\phi}_u | \hat{H} | \phi_u \bar{\phi}_i \phi_v \rangle}{\Delta E_{i \rightarrow t} + \Delta E_{v \rightarrow u}} \\
 &= \sum_i \frac{(uv|ti)(tv|ui)}{\varepsilon_i - \varepsilon_t + J_{uv}^C - J_{uu}^C} \quad (39)
 \end{aligned}$$

In summary, these contributions yield a correction of:

$$\begin{aligned}
 \Delta K_{tu} = & \sum_i \frac{(tu|vi)^2 - (tu|vi)(tv|ui)}{\varepsilon_i - \varepsilon_v + J_{tu}^C - J_{uu}^C} \\
 &+ \sum_i \frac{(tu|vi)^2 - (tu|vi)(uv|ti)}{\varepsilon_i - \varepsilon_v + J_{tu}^C - J_{tt}^C} \quad (40) \\
 &+ \sum_i \frac{(uv|ti)(tv|ui)}{\varepsilon_i - \varepsilon_t + J_{uv}^C - J_{uu}^C}.
 \end{aligned}$$

As can be seen in Fig. 11, the excited state determinant space of the additional 1p configurations is generated in the same way as for the additional 1h configurations: $\mathbb{S}^r = \{|\phi_u \bar{\phi}_u \phi_a\rangle, |\phi_t \bar{\phi}_t \phi_a\rangle, |\phi_t \phi_u \bar{\phi}_a\rangle\}$. Here, the corrections are given by:

$$\begin{aligned}
 (1) \quad & \sum_a \frac{\langle \phi_i \bar{\phi}_u \phi_v | \hat{H} | \phi_u \bar{\phi}_u \phi_a \rangle \langle \phi_u \bar{\phi}_u \phi_a | \hat{H} | \phi_u \bar{\phi}_i \phi_v \rangle}{\Delta E_{v \rightarrow a} + \Delta E_{i \rightarrow u}} \\
 &= \sum_a \frac{(tu|va)^2 - (tu|va)(uv|ta)}{\varepsilon_v - \varepsilon_a + J_{tu}^C - J_{uu}^C} \\
 (2) \quad & \sum_a \frac{\langle \phi_i \bar{\phi}_u \phi_v | \hat{H} | \phi_t \bar{\phi}_t \phi_a \rangle \langle \phi_t \bar{\phi}_t \phi_a | \hat{H} | \phi_u \bar{\phi}_i \phi_v \rangle}{\Delta E_{v \rightarrow a} + \Delta E_{u \rightarrow t}} \\
 &= \sum_a \frac{(tu|va)^2 - (tu|va)(tv|ua)}{\varepsilon_v - \varepsilon_a + J_{tu}^C - J_{tt}^C} \quad (41) \\
 (3) \quad & \sum_a \frac{\langle \phi_i \bar{\phi}_u \phi_v | \hat{H} | \phi_t \phi_u \bar{\phi}_a \rangle \langle \phi_t \phi_u \bar{\phi}_a | \hat{H} | \phi_u \bar{\phi}_i \phi_v \rangle}{\Delta E_{v \rightarrow a}} \\
 &= \sum_a \frac{(uv|ua)(tv|ta)}{\varepsilon_v - \varepsilon_a}
 \end{aligned}$$



1p: additional configurations for 3e-3c cases

Fig. 11 In the case of a 3c-3e system, three additional 1p configurations contribute to the exchange interaction.

which in total yields:

$$\begin{aligned}
 \Delta K_{tu} = & \sum_a \frac{(tu|va)^2 - (tu|va)(uv|ta)}{\varepsilon_v - \varepsilon_a + J_{tu}^C - J_{uu}^C} \\
 &+ \sum_a \frac{(tu|va)^2 - (tu|va)(tv|ua)}{\varepsilon_v - \varepsilon_a + J_{tu}^C - J_{tt}^C} \quad (42) \\
 &+ \sum_a \frac{(uv|ua)(tv|ta)}{\varepsilon_v - \varepsilon_a}
 \end{aligned}$$

Again, the energies of the excitations within the active space are given by the one-site repulsion energies instead of the orbital energies.

3.3 Summary of contributions

The contributions listed above are all effects that contribute to the effective exchange integral K_{tu} in a three-electron–three-centre case. Note that all off-diagonal elements of H , which correspond to single excitations, are approximated by the corresponding CASSCF Fock matrix elements. This approximation allows for a much easier implementation while the deviation from the actual off-diagonal elements of H may be expected to be small. Furthermore, we made another assumption by defining all energy differences of excitations within the active space by one-site repulsion energies instead of the orbital energies. Formally, this might be regarded as the usage of two different definitions for $\hat{H}^{(0)}$ depending on the orbital space, which may seem arbitrary as we deviate from the definition of $\hat{H}^{(0)}$ for charge polarised configurations. However, by using such an alternative definition of the energy differences within the active space the method gains a great deal of numerical stability since it avoids the most common causes of intruder states.

4 Implementation of the perturbational approach

The method for calculating the effective exchange integrals, described above, has been implemented into the ORCA program package.⁵⁶ The algorithm consists of the following steps:

(1) Generation of a set of molecular orbitals

The first step may seem trivial, but is crucial, as the molecular orbitals have a significant impact on the convergence of the perturbative approach. The method requires a CASSCF(n, n) calculation for the orbital generation.^{51,57} It is also essential that the generated molecular orbitals are canonical, since the subsequent steps are invalid otherwise.

(2) Localise the orbitals inside the active space

The localisation of the active orbitals is necessary to obtain the so-called ‘magnetic’ orbitals, as the Heisenberg approach relies on local spins, thus requiring localised orbitals. To fulfil this requirement, the New-Boys algorithm is employed.⁵⁸

(3) Calculation of the Fock matrix over molecular orbitals

This step underlines the necessity of starting with canonical orbitals, as they are indispensable for generating the Fock matrix over atomic orbitals with the following procedure. The canonical orbital energies correspond to the diagonal elements

of the diagonalised Fock matrix \mathbf{F}^{diag} . Here, the Fock matrix over atomic orbitals \mathbf{F}^{AO} is constructed using the coefficient matrix of the canonical orbitals \mathbf{C}^{old} along with the overlap matrix in the basis of atomic orbitals \mathbf{S} .

$$\mathbf{F}^{\text{AO}} = \mathbf{XY}^{\dagger}, \quad (43)$$

where:

$$\mathbf{X} = \mathbf{SC}^{\text{old}}, \quad (44)$$

$$\mathbf{Y} = \mathbf{SC}^{\text{old}} \mathbf{F}^{\text{diag}}. \quad (45)$$

The Fock matrix \mathbf{F}^{MO} of the new set of molecular orbitals with localised orbitals inside the active space is obtained using the coefficient matrix of the new set of orbitals \mathbf{C} :

$$\mathbf{F}^{\text{MO}} = \mathbf{C}^{\dagger} \mathbf{F}^{\text{AO}} \mathbf{C}. \quad (46)$$

In summary, the Fock operator is defined as the state-averaged CASSCF Fock operator^{51,52} (defined in Section 2) and the set of canonical molecular orbitals is assumed to diagonalise \hat{F}_{CASSCF} including the “internal-active” and “active-virtual” subspaces, which may not be necessarily true. Consequently, no contributions can be expected for the 1h and 1p excitations in case of two-spin systems. However, it simplifies the implementation.

(4) Transformation of the two-electron integrals

The conversion of two-electron integrals into the molecular orbital basis represents the most computationally demanding stage. However, the computational effort can be reduced notably as not all transformed integrals are essential for calculating K_{tu}^{eff} . By defining internal and virtual orbital windows, distinct integral classes can be derived. Incorporating active orbitals within both orbital windows enhances flexibility in selecting specific integrals from various classes. Within this implementation, only the $(ik|jl)$ and $(ia|jb)$ integral classes are computed.⁵⁹

Furthermore, the transformation is expedited by employing the “resolution of identity” (RI) approximation, which is mandatory in our implementation.⁵⁹ This necessitates the use of an auxiliary basis set that will be detailed below in the Results and discussion section. As a final and highly effective acceleration method, the “frozen core” approximation is employed. This technique excludes core orbitals from the transformation due to their minimal impact on the dynamic correlation energy, resulting in a substantial reduction in the integral transformation dimensionality and, with this, in significant computational time savings.

(5) Calculation of the effective exchange integrals

In the final step, the effective exchange integrals K_{tu}^{eff} are computed using the expressions from Section 3. Essentially, this involves calculating the matrix elements K_{tu} and their corrections. The output includes the first-order exchange matrix (including the K_{tu}), the individual second-order exchange matrices (including the $\Delta K_{tu}^{(2)}$), and the final exchange matrix (including the K_{tu}^{eff}), where the indices t and u iterate over the active orbitals. These matrices are always symmetric, and their dimension is determined by the number of electrons (or orbitals) in the CASSCF(n,n) calculation.

5 Results and discussion

5.1 Choice of molecules

Since our discussion focuses on (organic) multi-spin systems, we chose an organic diradical (1,3-(phenylene)bis(nitroxide)), an organic triradical (1,3,5-triphenylbenzenetriyltris(*N*-*tert*-butyl nitroxide)) and an anthracene–radical system (9-[3-(4,4,5,5-tetramethyl-1-yl oxyimidazolin-2-yl)phenyl]anthracene) to test the newly implemented method. The first two systems, shown on the left-hand side in Fig. 12, exhibit open-shell configurations in their ground state with known exchange coupling constants of $J = 695 \text{ cm}^{-1}$ and $J = 9.45 \text{ cm}^{-1}$.^{60,61} Note that the experimental value of the diradical was determined for the *N*-*tert*-butyl nitroxide. Here, we decided to truncate the *tert*-butyl groups in order to perform more accurate calculations. A benchmark on both of these systems, may also allow us to draw conclusions on the impact of the extent of the conjugated π -system. The latter system, depicted on the right-hand side in Fig. 12, forms an antiferromagnetically coupled open-shell system in its excited state.⁶² However, the magnitude of J for the anthracene system could not be determined experimentally, *i.e.* $J < 0 \text{ cm}^{-1}$.

5.2 Computational details

The geometries of the structures shown in Fig. 12 were optimised at the B3LYP/def2-TZVP level of theory.^{63–67} Since the DDPT2 method requires a common set of orbitals, we calculated the exchange interaction using only one structure (vertical excitation energy). Here, the calculations were accelerated by the RIJCOSX approximation using the def2/J auxiliary basis set.^{68,69}

The magnetic couplings are either obtained by our own implemented method or, in order to compare the results, by the FIC-NEVPT2 method using the def2-SVP basis set or variational methods such as DDCI3, DDCI2 or CASCI+S, where the singles “S” include the 1h, 1p and 1h-1p excitations, also using the def2-SVP basis set.^{26–28} The Fock matrix formations were accelerated by the RIJCOSX method using the def2/J auxiliary basis set and the integral transformations were accelerated by the RI method using the def2-SVP/C auxiliary basis set.

In general, the calculations are based on CASSCF(3,3) or CASSCF(2,2) zeroth-order wavefunctions (depending on the multiplicity). It is important to note that the convergence criteria were set to $E_{\text{Tol}} = 10^{-10}$ (energy gradient) and

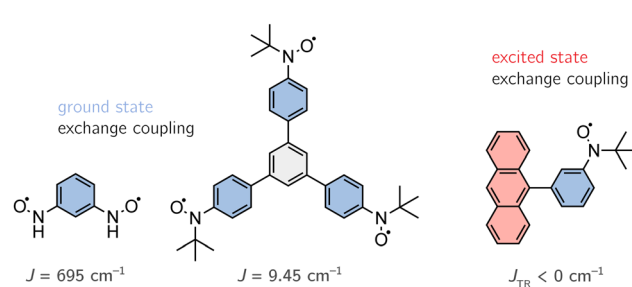


Fig. 12 Molecular structures of the chosen benchmark systems.

$g_{\text{Tot}} = 10^{-7}$ (orbital gradient), which is tight compared to the default settings in ORCA.

For the variational calculations, the selection parameter T_{sel} was set to zero in order to include all possible configuration state functions in the CI. The variational methods were always used in combination with a common set of molecular orbitals (Q_1 -optimised orbitals or T_1 -optimised orbitals).

The NEVPT2 calculations were performed state-specific, *i.e.* the quartet state and the trip-doublet state were optimised separately.

Our implementation relies on a common set of molecular orbitals, where we used differently optimised orbitals in a series of calculations. Since, in our implementation, only the effective exchange integrals K_{tu}^{eff} are computed, the exchange interaction J for the three-spin systems (or specifically referred to as J_{TR} in case of chromophore-radical systems) was calculated by $K_{tu}^{\text{eff}} + K_{uv}^{\text{eff}}$, where K_{tu}^{eff} and K_{uv}^{eff} are smaller in magnitude than K_{tv}^{eff} . In case of the two-spin system, J was calculated by $2K_{tu}^{\text{eff}}$.

5.3 Benchmark results for ground state radicals

Since experimental values for the exchange interaction are known for the nitroxide diradical and triradical ($J = 695 \text{ cm}^{-1}$ and $J = 9.45 \text{ cm}^{-1}$),^{60,61} these systems are well suited to compare the accuracy of the DDPT2 method to other multireference methods such as the variational DDCI3, DDCI2, and CASCI+S methods as well as the perturbational NEVPT2 method.

5.3.1 Choice of the computational methods. The variational methods are distinguished by their CI space: the DDCI3 method includes all possible excited state configurations except for the 2h-2p class of excited states, since these configurations do not affect the energy differences in second order perturbation theory. In the DDCI2 method, also the 2h-1p and 1h-2p excited states are omitted from the CI space, since they only introduce a non-negligible contribution to the energy difference for wavefunctions with larger amplitudes of the ionic forms. From a physical standpoint, the DDCI2 method compares best to the DDPT2 method, since both methods use the same determinant space. The CASCI+S method is even more approximate, omitting also the 2h and 2p excitations. However, as shown in the literature,⁴⁹ a CI with this particular space yields exchange interactions comparable to DDCI2 for conjugated, organic systems.

The NEVPT2 method is also chosen as a reference, since it is also a multi-reference second-order perturbation theory approach and is widely used for the calculation of exchange

coupling constants. The differences between the NEVPT2 method and the DDPT2 method are: (1) the choice of the zeroth-order Hamiltonian (Dyall's Hamiltonian in the NEVPT2 method),⁷⁰ (2) the inclusion of all possible excitation classes in the NEVPT2 method, which can be generated by single and double excitations, and (3) the fact that the NEVPT2 method relies on a contracted description of the first-order wavefunction, which is not the case for the DDPT2 method. Here, we will only use the fully-internally contracted NEVPT2 method (FIC-NEVPT2).

Since the DDPT2 method requires a common orbital basis, it makes sense to tailor the orbital optimisation to the ground state radicals and then to apply a corresponding protocol to the anthracene system.

5.3.2 Calculations on the nitroxide diradical. First, we will focus on the nitroxide diradical. Table 1 lists the exchange interaction J for the diradical calculated at different levels of theory using different sets of orbitals. As can be seen, all used methods predict the correct sign of J . However, depending on the method, vastly different magnitudes of J are obtained. Starting at zeroth-order, *i.e.* at the CASSCF(2,2) level of theory (with triplet-optimised orbitals), a J of 126 cm^{-1} is calculated, which underestimates the exchange interactions by a factor of 5.5; the necessity to consider excited determinants for a more accurate description of J thus becomes evident. As already shown in the literature for the exact same system,⁴⁹ the inclusion of all singly excited states with reference to the CASCI, *i.e.* the 1h, 1p and 1h-1p excitations, constitutes the main contribution to the exchange interaction for this system. By coincidence, this method even yields a value for the exchange coupling that is slightly closer to the experimentally deduced value than the other methods considered here. Consequently, the dynamic spin polarisation and the dynamic charge polarisation effects, including their relaxation through the 1h and 1p excitations, may be considered as the most important effects for J regarding this conjugated organic compound. However, this shall not imply, that CASCI+S is the best choice when it comes to the calculation of the exchange interaction in conjugated organic compounds. Due to the narrow FOIS (only 1h and 1p and 1h-1p determinants), unsystematic deviations from the actual value of J might arise.

When the 2h and 2p excited determinants are introduced additionally (DDCI2), a slight decrease of J by -33 cm^{-1} can be observed, which means that the 2h and 2p excited states have a rather small anti-ferromagnetic effect on J . The additional

Table 1 Calculated J values for the nitroxide diradical using different levels of theory. In general, the calculations are based on CASSCF(2,2) zeroth-order wavefunctions with different weights w for the ionic forms in the orbital optimisation

	CASSCF(2,2)	DDCI3	DDCI2	CASCI+S	FIC-NEVPT2	DDPT2	Exp.
$w = 0$	126	657	647	680	172	169	695
$w = 0.133$	634				438	722	
State-specific	122				482		
ROHF ^a	104	649	629	658	154	140	

^a An additional series of calculations were performed with orbitals from a ROHF calculation on the open-shell singlet state. All values are given in cm^{-1} .



inclusion of the 1h-2p and 2h-1p excited states (DDCI3) increases the J value by 10 cm^{-1} compared to the DDCI2 value. The contributions of the 2h-1p and 1h-2p excited states cancel each other out.⁴⁹

The FIC-NEVPT2 method, using the triplet-optimised orbitals, yields a J value of 172 cm^{-1} , which compares well to the DDPT2 value of $J(w=0) = 169\text{ cm}^{-1}$, where w is the weight of the ionic determinants in the CASSCF procedure. Both methods underestimate the exchange interaction severely indicating that the coupling of the FOIS functions among themselves (that come in at fourth and higher orders in perturbation theory) plays an important role, as discussed in depth by Calzado and Malrieu.^{21,44}

However, the choice of orbitals also plays an important role, in particular in low order perturbation theory. In fact, NEVPT2 with state-specifically optimised orbitals yields a coupling of $J_{\text{NEVPT2(SS)}} = 482\text{ cm}^{-1}$. However, the coupling is still underestimated as higher-order effects are missing.

The use of orbitals from a ROHF calculation for the open-shell singlet state and the use of triplet-optimised orbitals yields almost identical results, since the same electronic configuration is modeled in both approaches.

It is known that the exchange interaction is strongly underestimated in multi-reference perturbation theory methods with minimal active space zeroth-order wavefunctions when the orbital optimisation primarily considers neutral determinants. The resulting orbitals are too compact; the exchange interaction can only be described well through higher-order interactions. As discussed by Angeli and co-workers,⁵³ the charge polarising effect of the higher order terms can be crudely simulated by optimising a singlet CASSCF(2,2) wavefunction and artificially giving a higher weight to the ionic states (the second and third singlet roots) in the orbital optimisation. The increased weight of the ionic states then leads the optimisation to converge to more diffuse orbitals, which, subsequently, provides improved values for the exchange interaction at low orders of perturbation.⁵³

Fig. 13 illustrates the dependence of the calculated exchange interaction and its individual contributions on the weight w of the ionic states in the orbital optimisation. The calculations

were performed for the diradical using the DDPT2 method. In the case of this system, the exchange coupling is barely influenced by the kinetic exchange (KE) contribution.

The 1h and 1p contributions are strictly zero for two-spin systems as we approximated the single-excitation Hamiltonian matrix elements by the SA-CASSCF Fock matrix elements, which we assumed to be diagonal.

Fig. 13 shows a strong (non-linear) dependence of J on w . To obtain accurate and meaningful J -values, the challenge will be to identify a suitable weight w which is *a priori* not known and will differ for systems of different size and nature. However, if the exchange interaction is known experimentally for a particular system, the distinct trend observed as a function of w will make it possible to identify an appropriate weighting factor that should allow us to calculate accurate J -values for a whole series of similar systems. For the diradical, a weight of 0.133 provides good orbitals for the calculation of J , where a value of $J(w=0.133) = 722\text{ cm}^{-1}$ is obtained, in good agreement with the experimental value of 695 cm^{-1} .

A FIC-NEVPT2 calculation using the same weight of $w = 0.133$ yields an exchange coupling constant of $J_{\text{NEVPT2}}(w = 0.133) = 438\text{ cm}^{-1}$, which is smaller in magnitude than the DDPT2 value with the same ionic weight and even smaller than the corresponding CASSCF(2,2) value of 634 cm^{-1} . The main reason for this deviation is the contribution of the 1h and 1p determinants in the NEVPT2 method, which are not taken into account in the DDPT2 method. The 1h and 1p determinants lead to an orbital relaxation and tend to act in favour of the singlet state. Interestingly, the effect of this orbital relaxation can become so large, that even a wrong sign can be predicted as illustrated in Fig. 14, showing the trend of the computed J values against w for DDPT2 and NEVPT2. For example, when using NEVPT2 with an ionic weight of $w = 0.4$, a coupling of $J_{\text{NEVPT2}}(w = 0.4) = -2.4\text{ cm}^{-1}$ is obtained. Consequently, one needs to be careful with state-averaging when using, for example, the NEVPT2 method. The current implementation of the DDPT2 method circumvents this problem intrinsically by assuming the SA-CASSCF Fock matrix to be diagonal.

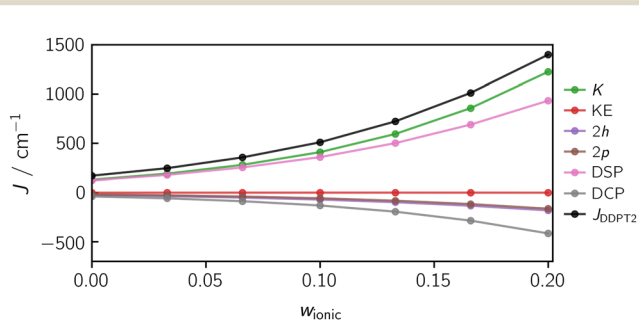


Fig. 13 The calculated exchange coupling constant J using the DDPT2 method for the diradical as a function of the weight w of the ionic determinants in the orbital optimisation. The individual effects exhibit a non-linear dependence on w . Here, an optimal results for J corresponds to an ionic weight of $w = 0.133$.

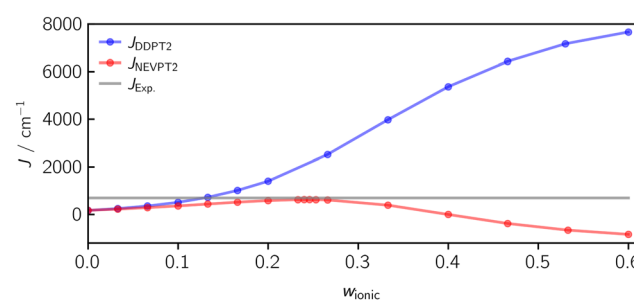


Fig. 14 The computed J value against the ionic weight w using the DDPT2 and the NEVPT2 methods. While for the DDPT2 method, the J -values converge to an upper bound with the correct (positive) sign, the J values converge to a lower bound for the NEVPT2 method with a negative sign, due to the orbital relaxation. The optimal weight using the NEVPT2 method is larger compared to the DDPT2 method and localised at the maximum in case of the ferromagnetically coupled diradical.



Using the DDPT2 method, the J -values increase monotonically with w and converge to an upper bound. Using the NEVPT2 method, the values go through a local maximum and then converge to a negative value of J , due to the orbital relaxation. Interestingly, the most accurate J value for the NEVPT2 method is obtained at the maximum of the curve with $J_{\text{NEVPT2}}(w = 0.246) = 625 \text{ cm}^{-1}$. However, the exact value is not reached. In future work, it may be worth investigating if this is a general behaviour of the NEVPT2 method for ferromagnetically coupled compounds.

5.3.3 Calculations on the nitroxide triradical. Further benchmark calculations have been carried out on the nitroxide triradical of Fig. 12. The computed J -values are listed in Table 2. Here, only DDPT2 and FIC-NEVPT2 calculations were performed, since, any variational calculations become already very expensive for molecules of this size, especially when choosing a selection threshold of $T_{\text{sel}} = 0$. As for the smaller diradical, the J -values are severely underestimated for $w = 0$, whereby the effect is even more drastic for the triradical: one obtains $J_{\text{DDPT2}}(w = 0) = 0.283 \text{ cm}^{-1}$ and $J_{\text{NEVPT2}}(w = 0) = 0.497 \text{ cm}^{-1}$. A state-specific FIC-NEVPT2 calculation does not yield a significant improvement with $J_{\text{NEVPT2}}(\text{SS}) = 0.741 \text{ cm}^{-1}$.

To achieve a result with the DDPT2 method, that is relatively close to the experimental value of 9.45 cm^{-1} , one might choose an ionic weight of $w = 0.375$, which yields a J value of $J_{\text{DDPT2}}(w = 0.375) = 11.4 \text{ cm}^{-1}$. A FIC-NEVPT2 calculation with the same weight yields $J_{\text{NEVPT2}}(w = 0.375) = 6.00 \text{ cm}^{-1}$, where the J -value is again damped by the anti-ferromagnetic orbital relaxation through the 1h and 1p determinants. This observation suggests that, for ferromagnetically-coupled systems, the optimal weight in state-averaged NEVPT2 calculations will be higher compared to the DDPT2 method. In case of antiferromagnetically-coupled systems, the optimal weight may be smaller compared to the DDPT2 method.

Comparing the optimal weights w for the triradical and the diradical, one finds that the optimal ionic weight may correlate with the system size, *i.e.* with the size of the π system. In order to calculate an accurate J value for a larger π system, a larger ionic weight w is likely to be necessary. The reason for this might be, that, in large π -systems, the ionic forms are better stabilised through the enhanced delocalisation. Now, if one increases w , only a slight expansion of the magnetic orbitals will be observed. This means, that, in case of a smaller π system, the relaxation of the ionic forms has to be connected with a larger expansion of the magnetic orbitals, which will lead to much more expanded orbitals at a smaller w .

Table 2 Calculated J values for the nitroxide triradical using the DDPT2 method and the FIC-NEVPT2 method. In general, the calculations are based on CASSCF(3,3) zeroth-order wavefunctions with different weights w for the ionic forms in the orbital optimisation. All values are given in cm^{-1}

	CASSCF(3,3)	FIC-NEVPT2	DDPT2	Exp.
$w = 0$	0.191	0.497	0.283	9.45
$w = 0.375$	5.87	6.00	11.4	
State-specific	0.190	0.741		

5.4 Scaling of the DDPT2 method

The most elaborate step of the DDPT2 method is the transformation of the two-electron integrals. Only the $(ik|jl)$ and $(ia|jb)$ integrals are required for the computation of the effective exchange integrals. Therefore, in an optimal implementation, the computation time t should scale as follows:

$$t = m \cdot N \cdot (N_{\text{int}}^4 + N_{\text{int}}^2 N_{\text{virt}}^2), \quad (47)$$

where N is the number of basis functions, N_{int} is the number of internal orbitals, N_{virt} is the number of virtual orbitals and m is a constant factor. Since $N = N_{\text{int}} + N_{\text{virt}}$, we can rewrite this equation as:

$$t = m \cdot N N_{\text{int}}^2 \cdot (N^2 - 2NN_{\text{int}} + 2N_{\text{int}}^2). \quad (48)$$

Introducing the ratio $c = N_{\text{int}}/N$, we obtain:

$$t = m \cdot (c^2 - 2c^3 + 2c^4)N^5. \quad (49)$$

As a consequence, the DDPT2 method should scale as N^5 . The term inside the brackets alters t by a factor, which can take values between zero and one. In case of $N_{\text{int}} = N$, the computation time scales exactly as N^5 . Although the RI approximation is invoked, the scaling of the method is not reduced, only the pre-factor. This is expected since the construction of the RI integrals scales as N^4 but the assembly of the final four index integrals from the RI integrals is a N^5 step, albeit with a small pre-factor.

To validate the above equation, 20 calculations were carried out, where, in each successive calculation, a xenon atom was added. This ensures that the ratio c remains constant. The calculations were performed using the def2-TZVP basis set and the def2-SVP/C auxiliary basis set. The computational time t as a function of the basis functions N is depicted in Fig. 15. With 8 cores (Apple M2 Max) and 8 GB of RAM per core, a computation time of 549.5 s was obtained for 920 basis functions (1000 basis functions including frozen core orbitals). Thus, medium to large systems (depending on the basis set size) can be calculated within a short time frame. The computation times were fitted with a function of the form: $t = m \cdot N^x$, yielding a pre-factor of $m = 4.69 \times 10^{-12} \text{ s}$ and an exponent of $x \approx 4.75$. The exponent determined here approximately confirms the

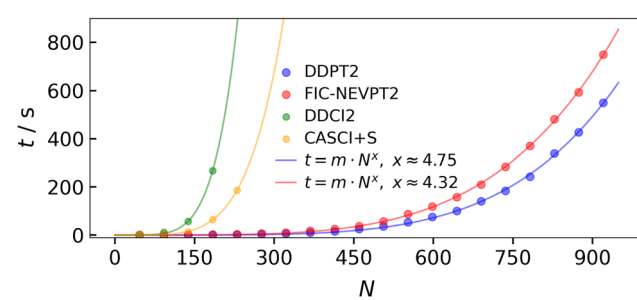


Fig. 15 Computation time t (actual values and fitted values) against the number of basis functions N for the DDPT2, NEVPT2, DDCI2 and CASCI+S method. Note that the number of frozen core orbitals are subtracted from N . The calculations were carried out using 8 cores (Apple M2 Max) with 8 GB of RAM per core.

theoretically expected exponent of $x = 5$. The scaling of the DDPT2 method was also compared to the FIC-NEVPT2 method. In order to calculate the exchange interaction using the NEVPT2 method, two states need to be computed to obtain a meaningful comparison between the DDPT2 and NEVPT2 methods. Note that the RI approximation was also invoked in the FIC-NEVPT2 calculations. Using the same fit function as for the DDPT2 method, a scaling factor of $x \approx 4.32$ was obtained. The scaling factor obtained for the FIC-NEVPT2 method is better than that of the DDPT2 method. However, the pre-factor is much larger with $m = 1.21 \times 10^{-10}$ s. As a consequence, it is expected that the DDPT2 method is faster for small and medium sized systems, whereas the FIC-NEVPT2 method should be faster for larger systems, due to its contracted nature.

The variational treatment of the exact same determinant space as in the DDPT2 method leads to the DDCI2 method. However, as can be seen in Fig. 15, the variational treatment becomes quickly unfeasible with an increasing number of basis functions making perturbational methods much more attractive for larger systems. Even with a smaller FOIS, such as that of the CASCI+S method, the scaling is still very steep compared to the perturbational methods.

The reason for the very large pre-factors of the DDCI2 and CASCI+S methods is largely of a technical nature since in the ORCA MRCI program matrix elements are being calculated one at a time which is far less efficient than constructing the sigma-vector through a series of matrix multiplications that only require a subset of the molecular integrals in each contraction. The reason for the ORCA implementation not following such an approach is that the program gains efficiency through individual selection, which interferes with a matrix driven construction. Secondly, a matrix driven, uncontracted MRCI approach is of high technical complexity and has, so far, not been attempted in the ORCA program. However, an internally contracted DDCI implementation has been available in ORCA since 2016 and will be numerically evaluated in a subsequent study.

5.5 A case study on the anthracene–radical system

In the orbital optimisation of the anthracene radical system, we used a weighting of the ionic states of $w = 0.375$, just as for the nitroxide triradical. This w should yield good values for J if the insights gained from the orbital optimisation of the nitroxide triradical, *i.e.* w depends on the size of the π -system, are applicable to the anthracene radical system.

Calculations were performed using the def2-SVP and def2-TZVP basis sets to ascertain the dependence of the result on the basis set size. The obtained values are $J_{\text{DDPT2}}(w = 0.375, \text{def2-SVP}) = -4.76 \text{ cm}^{-1}$ and $J_{\text{DDPT2}}(w = 0.375, \text{def2-TZVP}) = -5.01 \text{ cm}^{-1}$. The results do not differ significantly and have

the correct sign, suggesting that the calculated value of J is less dependent on the basis set size but more on the method used.

A FIC-NEVPT2 calculation with the same weight yields a value of $J_{\text{NEVPT2}}(w = 0.375) = -6.27 \text{ cm}^{-1}$. This confirms the assumption that, for antiferromagnetic system, the NEVPT2 method should yield larger couplings than the DDPT2 method when considering the same w . Furthermore, the 2h-1p and 1h-2p contributions in the NEVPT2 method give a total contribution of -0.313 cm^{-1} justifying a perturbational treatment using only the DDCI2 space, as carried out within the DDPT2 method.

A DDCI2 calculation on this system with Q_1 -optimised orbitals using the def2-SVP basis set gave an exchange coupling constant of $J_{\text{DDCI2}} = -6.14 \text{ cm}^{-1}$, which is in good agreement. Since DDCI2 can yield excellent values for the exchange interaction in organic systems, as shown by Calzado *et al.* and Barone *et al.*^{49,71} we might expect the calculated values to be close to the exact value of J_{TR} .

For the further discussion, only $J_{\text{DDPT2}}(w = 0.375, \text{def2-SVP})$ will be used. Table 3 summarises all individual second-order contributions to the exchange interaction J_{TR} . Here, the direct exchange sums up to 2.02 cm^{-1} . The kinetic exchange contribution, which is often used to explain the negative sign of the exchange interaction, does only (almost) cancel out the direct exchange with a contribution of -1.93 cm^{-1} .³³ CASSCF(3,3) yields a J value of 0.313 cm^{-1} , which approximately matches the result from the DDPT2 method, where only the direct and kinetic exchange contributions are included ($J = 0.094 \text{ cm}^{-1}$). This indicates that eqn (25) for calculating the kinetic exchange remains valid for this system, even though the equation is strictly only valid in the case of two degenerate orbitals.

The most important contribution stems from the dynamic spin polarisation effect with an anti-ferromagnetic contribution of -4.09 cm^{-1} . Since this contribution is much larger than the direct exchange, its sign determines the sign of the final exchange interaction J_{TR} . Assuming the dynamic spin polarisation to be equally important for other chromophore–radical systems, the sign of the exchange interaction J_{TR} could be qualitatively predicted by predicting the sign of the dynamic spin polarisation contribution. All other second order contributions are small compared to the kinetic exchange and the dynamic spin polarisation and act in favour of the doublet state (*i.e.* anti-ferromagnetic coupling).

6 Conclusion

The DDPT2 implementation reported in this work is based on the perturbational approach by de Loth, *et al.* and allows for the direct calculation of the effective exchange integrals.²² The method seems to be promising for the calculation of exchange

Table 3 Summary of the individual contributions to the exchange interaction J_{TR} for the anthracene–radical system

$K_{ab} + K_{bc}$	KE	1ö	1p	2h	2p	DSP	DCP	J_{TR}
2.02 cm^{-1}	-1.93 cm^{-1}	$\approx 0 \text{ cm}^{-1}$	$\approx 0 \text{ cm}^{-1}$	-0.314 cm^{-1}	-0.166 cm^{-1}	-4.09 cm^{-1}	-0.265 cm^{-1}	-4.67 cm^{-1}

interactions of medium- and large-sized organic molecules ($O(N^5)$ scaling) in combination with molecular orbitals generated from state-averaged CASSCF calculations. We could show a non-linear dependence of the calculated J -value on the weight w of the ionic determinants in the orbital optimisation procedure of the CASSCF calculation. If the optimal weight for a specific system is known, it should, in principle, be possible to calculate accurate values for the exchange interaction for a series of similar molecules. The dependence of the J value on the ionic weight w might be seen as a drawback of the DDPT2 method. However, it is not a unique problem to the DDPT2 method but a common problem for low-order MRPT methods in general.

The benchmark on the ground state radicals showed, that the optimal ionic weight w depends on the size of the conjugated π -system, where w increases with the size of the π system. In the case of the smaller diradical, the J -value was calculated to be $J_{\text{DDPT2}}(w = 0.133) = 722 \text{ cm}^{-1}$, which is close to the experimental value of 695 cm^{-1} . In the case of the triradical, the J -value was calculated to be $J_{\text{DDPT2}}(w = 0.375) = 11.4 \text{ cm}^{-1}$, which is also in good agreement with the experimental value of 9.45 cm^{-1} . The same weight as for the triradical was used in the calculation of the exchange interaction for the anthracene-radical system, where a value of $J(w = 0.375) = -4.67 \text{ cm}^{-1}$ was calculated, which is in good agreement with the DDCI2 value of -6.14 cm^{-1} . Thus, we might expect the calculated result to be close to the exact value for the exchange interaction.^{48,49}

In principle, it is also possible to obtain similar results for J_{TR} with the NEVPT2 method when using molecular orbitals generated from state-averaged CASSCF calculations. However, DDPT2 allows the separation of the dynamic spin polarisation contribution from the dynamic charge polarisation contribution, which is very useful for the investigation of important exchange mechanisms. Using the DDPT2 method, we could show that the dynamic spin polarisation effect is significantly more important than the dynamic charge polarisation contribution (and all other contributions) in case of the photogenerated triplet–doublet system investigated in this work. This observation is likely applicable to other photoexcited chromophore–radical systems. Consequently, to predict the sign of the exchange interaction J_{TR} qualitatively, one needs to be able to predict the sign of the dynamic spin polarisation effect in a qualitative manner,⁵⁵ which will be the focus of our future work.

Regarding the DDPT2 method, future work will focus on (1) a less approximate treatment of the single excitations, which allows us to take the orbital relaxation through the 1h and 1p determinants into account. This way, a more accurate trend of the exchange interaction against w can be obtained, especially for ferromagnetically-coupled systems. (2) It should be investigated which higher-order effects have a significant effect on the exchange interaction in organic compounds. Here, the dynamic spin polarisation is likely to play an important role. (3) The reference space in the DDPT2 method may be expanded to a complete active space. However, only a minor improvement to the calculated exchange interaction might be expected for many organic compounds. (4) The usage of Dyall's Hamiltonian as $\hat{H}^{(0)}$ will allow us to drop the approximations made in the

derivation of the working equations, *i.e.* introducing two-electron interactions in case of charge-polarised active spaces. This way, a less approximate calculation strategy can be obtained.

Author contributions

Implementation of the code, quantum chemical calculations, investigation, methodology, formal analysis, data validation and visualisation, original draft writing M. F.; implementation, supervision, review and editing of the manuscript F. N.; conceptualisation, project administration, funding acquisition, supervision, review and editing of the manuscript S. R.

Data availability

The data supporting the findings of this study are available within the article.

Conflicts of interest

There are no conflicts to declare.

Acknowledgements

This work was supported by the Deutsche Forschungsgemeinschaft (DFG, German Research Foundation) – Project numbers 417643975 and 536668010 (S. R.). The authors acknowledge support by the state of Baden-Württemberg through bwHPC and the German Research Foundation (DFG) through grant no INST 40/575-1 FUGG (JUSTUS 2 cluster). F. N. would like to thank the Max Planck Society for financial support. Open Access funding provided by the Max Planck Society.

Notes and references

- 1 T. Quintes, M. Mayländer and S. Richert, *Nat. Rev. Chem.*, 2023, **7**, 75–90.
- 2 R. J. Hudson, T. S. C. MacDonald, J. H. Cole, T. W. Schmidt, T. A. Smith and D. R. McCamey, *Nat. Rev. Chem.*, 2024, **8**, 136–151.
- 3 S. Bayliss, D. Laorenza, P. Mintun, B. Kovos, D. Freedman and D. Awschalom, *Science*, 2020, **370**, 1309–1312.
- 4 S. Sanvito, *Chem. Soc. Rev.*, 2011, **40**, 3336–3355.
- 5 M. Mayländer, S. Chen, E. R. Lorenzo, M. R. Wasielewski and S. Richert, *J. Am. Chem. Soc.*, 2021, **143**, 7050–7058.
- 6 J. N. Nelson, J. Zhang, J. Zhou, B. K. Rugg, M. D. Krzyaniak and M. R. Wasielewski, *J. Chem. Phys.*, 2020, **152**, 014503.
- 7 J. H. Olshansky, J. Zhang, M. D. Krzyaniak, E. R. Lorenzo and M. R. Wasielewski, *J. Am. Chem. Soc.*, 2020, **142**, 3346–3350.
- 8 Y. Qiu, A. Equbal, C. Lin, Y. Huang, P. J. Brown, R. M. Young, M. D. Krzyaniak and M. R. Wasielewski, *Angew. Chem., Int. Ed.*, 2023, **62**, e202214668.



9 S. Gorgon, K. Lv, J. Grüne, B. H. Drummond, W. K. Myers, G. Londi, G. Ricci, D. Valverde, C. Tonnelé, P. Murto, A. S. Romanov, D. Casanova, V. Dyakonov, A. Sperlich, D. Beljonne, Y. Olivier, F. Li, R. H. Friend and E. W. Evans, *Nature*, 2023, **620**, 538–544.

10 M. Mayländer, K. Kopp, O. Nolden, M. Franz, P. Thielert, A. Vargas Jentzsch, P. Gilch, O. Schiemann and S. Richert, *Chem. Sci.*, 2023, **14**, 10727–10735.

11 M. Mayländer, P. Thielert, T. Quintes, A. Vargas Jentzsch and S. Richert, *J. Am. Chem. Soc.*, 2023, **145**, 14064–14069.

12 A. Yamauchi, K. Tanaka, M. Fuki, S. Fujiwara, N. Kimizuka, T. Ryu, M. Saigo, K. Onda, R. Kusumoto, N. Ueno, H. Sato, Y. Kobori, K. Miyata and N. Yanai, *Sci. Adv.*, 2024, **10**, eadi3147.

13 R. M. Jacobberger, Y. Qiu, M. L. Williams, M. D. Krzyaniak and M. R. Wasielewski, *J. Am. Chem. Soc.*, 2022, **144**, 2276–2283.

14 Y. Qiu, H. J. Eckvahl, A. Equbal, M. D. Krzyaniak and M. R. Wasielewski, *J. Am. Chem. Soc.*, 2023, **145**, 25903–25909.

15 S. L. Bayliss, P. Deb, D. W. Laorenza, M. Onizhuk, G. Galli, D. E. Freedman and D. D. Awschalom, *Phys. Rev. X*, 2022, **12**, 031028.

16 E. M. Giacobbe, Q. Mi, M. T. Colvin, B. Cohen, C. Ramanan, A. M. Scott, S. Yeganeh, T. J. Marks, M. A. Ratner and M. R. Wasielewski, *J. Am. Chem. Soc.*, 2009, **131**, 3700–3712.

17 M. T. Colvin, E. M. Giacobbe, B. Cohen, T. Miura, A. M. Scott and M. R. Wasielewski, *J. Phys. Chem. A*, 2010, **114**, 1741–1748.

18 M. T. Colvin, A. L. Smeigh, E. M. Giacobbe, S. M. M. Conron, A. B. Ricks and M. R. Wasielewski, *J. Phys. Chem. A*, 2011, **115**, 7538–7549.

19 S. Weber, *eMagRes*, 2017, **6**, 255–270.

20 M. Franz, F. Neese and S. Richert, *Chem. Sci.*, 2022, **13**, 12358–12366.

21 J. P. Malrieu, R. Caballol, C. J. Calzado, C. De Graaf and N. Guihery, *Chem. Rev.*, 2014, **114**, 429–492.

22 P. De Loth, P. Cassoux, J. Daudey and J. Malrieu, *J. Am. Chem. Soc.*, 1981, **103**, 4007–4016.

23 J. P. Malrieu, P. Claverie and S. Diner, *Theor. Chim. Acta*, 1967, **8**, 404–423.

24 J. Miralles, J.-P. Daudey and R. Caballol, *Chem. Phys. Lett.*, 1992, **198**, 555–562.

25 J. Miralles, O. Castell, R. Caballol and J.-P. Malrieu, *Chem. Phys.*, 1993, **172**, 33–43.

26 C. Angeli, R. Cimiraglia, S. Evangelisti, T. Leininger and J.-P. Malrieu, *J. Chem. Phys.*, 2001, **114**, 10252–10264.

27 C. Angeli, R. Cimiraglia and J.-P. Malrieu, *Chem. Phys. Lett.*, 2001, **350**, 297–305.

28 C. Angeli, R. Cimiraglia and J.-P. Malrieu, *J. Chem. Phys.*, 2002, **117**, 9138–9153.

29 K. Andersson, P.-Å. Malmqvist and B. O. Roos, *J. Chem. Phys.*, 1992, **96**, 1218–1226.

30 P. A. M. Dirac, *Proc. R. Soc. London, Ser. A*, 1926, **112**, 661–677.

31 W. Heisenberg, *Original Scientific Papers/Wissenschaftliche Originalarbeiten*, Springer, 1985, pp. 580–597.

32 J. H. Van Vleck, *Theory of Electric and Magnetic Susceptibilities*, Clarendon Press, Oxford, 1932.

33 C. De Graaf and R. Broer, *Magnetic Interactions in Molecules and Solids*, Springer, Cham, 2016.

34 R. L. Ake and M. Gouterman, *Theor. Chim. Acta*, 1969, **15**, 20–42.

35 M. G. Cory and M. C. Zerner, *Chem. Rev.*, 1991, **91**, 813–822.

36 F. Nepveu, W. Haase and H. Astheimer, *J. Chem. Soc., Faraday Trans. 2*, 1986, **82**, 551–565.

37 P. De Loth, P. Karafiloglou, J. P. Daudey and O. Kahn, *J. Am. Chem. Soc.*, 1988, **110**, 5676–5680.

38 P. de Loth, J.-P. Daudey, H. Astheimer, L. Walz and W. Haase, *J. Chem. Phys.*, 1985, **82**, 5048–5052.

39 H. Astheimer and W. Haase, *J. Chem. Phys.*, 1986, **85**, 1427–1432.

40 K. Handrick, J. P. Malrieu and O. Castell, *J. Chem. Phys.*, 1994, **101**, 2205–2212.

41 O. Castell, R. Caballol, V. Garcia and K. Handrick, *Inorg. Chem.*, 1996, **35**, 1609–1615.

42 J. Cabrero, N. Ben Amor, C. De Graaf, F. Illas and R. Caballol, *J. Phys. Chem. A*, 2000, **104**, 9983–9989.

43 C. J. Calzado, J. F. Sanz and J. P. Malrieu, *J. Chem. Phys.*, 2000, **112**, 5158–5167.

44 C. J. Calzado, C. Angeli, D. Taratiel, R. Caballol and J.-P. Malrieu, *J. Chem. Phys.*, 2009, **131**, 044327.

45 O. Castell and R. Caballol, *Inorg. Chem.*, 1999, **38**, 668–673.

46 J. Cabrero, N. Ben-Amor and R. Caballol, *J. Phys. Chem. A*, 1999, **103**, 6220–6224.

47 I. Negodaev, C. de Graaf and R. Caballol, *Chem. Phys. Lett.*, 2008, **458**, 290–294.

48 V. Barone, I. Cacelli, P. Cimino, A. Ferretti, S. Monti and G. Prampolini, *J. Phys. Chem. A*, 2009, **113**, 15150–15155.

49 C. J. Calzado, C. Angeli, C. de Graaf and R. Caballol, *Theor. Chem. Acc.*, 2011, **128**, 505–519.

50 F. Illas, I. P. Moreira, C. De Graaf and V. Barone, *Theor. Chem. Acc.*, 2000, **104**, 265–272.

51 B. O. Roos, P. R. Taylor and P. E. Sigbahn, *Chem. Phys.*, 1980, **48**, 157–173.

52 B. O. Roos, *Int. J. Quantum Chem.*, 1980, **18**, 175–189.

53 C. Angeli and C. J. Calzado, *J. Chem. Phys.*, 2012, **137**, 034104.

54 A. Szabo and N. S. Ostlund, *Modern Quantum Chemistry: Introduction to Advanced Electronic Structure Theory*, Courier Corporation, 2012.

55 P. Karafiloglou, *J. Chem. Educ.*, 1989, **66**, 816.

56 F. Neese, *Wiley Interdiscip. Rev.: Comput. Mol. Sci.*, 2022, **12**, e1606.

57 C. Kollmar, K. Sivalingam, B. Helmich-Paris, C. Angeli and F. Neese, *J. Comput. Chem.*, 2019, **40**, 1463–1470.

58 S. F. Boys, *Rev. Mod. Phys.*, 1960, **32**, 296.

59 F. Neese, *J. Comput. Chem.*, 2023, **44**, 381–396.

60 T. Ishida and H. Iwamura, *J. Am. Chem. Soc.*, 1991, **113**, 4238–4241.

61 H. Iwamura, K. Inoue and N. Koga, *New J. Chem.*, 1998, **22**, 201–210.

62 Y. Teki, S. Miyamoto, M. Nakatsuji and Y. Miura, *J. Am. Chem. Soc.*, 2001, **123**, 294–305.

63 A. D. Becke, *J. Chem. Phys.*, 1993, **98**, 1372–1377.

64 C. Lee, W. Yang and R. G. Parr, *Phys. Rev. B: Condens. Matter Mater. Phys.*, 1988, **37**, 785.



65 S. H. Vosko, L. Wilk and M. Nusair, *Can. J. Phys.*, 1980, **58**, 1200–1211.

66 P. J. Stephens, F. J. Devlin, C. F. Chabalowski and M. J. Frisch, *J. Phys. Chem.*, 1994, **98**, 11623–11627.

67 F. Weigend and R. Ahlrichs, *Phys. Chem. Chem. Phys.*, 2005, **7**, 3297–3305.

68 F. Neese, F. Wennmohs, A. Hansen and U. Becker, *Chem. Phys.*, 2009, **356**, 98–109.

69 F. Weigend, *Phys. Chem. Chem. Phys.*, 2006, **8**, 1057–1065.

70 K. G. Dyall, *J. Chem. Phys.*, 1995, **102**, 4909–4918.

71 V. Barone, I. Cacelli and A. Ferretti, *Phys. Chem. Chem. Phys.*, 2018, **20**, 18547–18555.